A diamond-based scanning probe spin sensor operating at low temperature in ultra-high vacuum

E. Schaefer-Nolte, F. Reinhard, M. Ternes', J. Wrachtrup, and K. Kern

Citation: Review of Scientific Instruments **85**, 013701 (2014); doi: 10.1063/1.4858835
View online: http://dx.doi.org/10.1063/1.4858835
View Table of Contents: http://aip.scitation.org/toc/rsi/85/1
Published by the American Institute of Physics

A diamond-based scanning probe spin sensor operating at low temperature in ultra-high vacuum

E. Schaefer-Nolte,[1,2] F. Reinhard,[2] M. Ternes,[1,a)] J. Wrachtrup,[1,2] and K. Kern[1,3]
[1]*Max-Planck Institute for Solid State Research, 70569 Stuttgart, Germany*
[2]*3rd Institute of Physics and Research Center SCoPE, University Stuttgart, 70569 Stuttgart, Germany*
[3]*Institut de Physique de la Matière Condenseé, Ecole Polytechnique Fédérale de Lausanne, 1015 Lausanne, Switzerland*

(Received 17 October 2013; accepted 13 December 2013; published online 8 January 2014)

We present the design and performance of an ultra-high vacuum (UHV) low temperature scanning probe microscope employing the nitrogen-vacancy color center in diamond as an ultrasensitive magnetic field sensor. Using this center as an atomic-size scanning probe has enabled imaging of nanoscale magnetic fields and single spins under ambient conditions. In this article we describe an experimental setup to operate this sensor in a cryogenic UHV environment. This will extend the applicability to a variety of molecular systems due to the enhanced target spin lifetimes at low temperature and the controlled sample preparation under UHV conditions. The instrument combines a tuning-fork based atomic force microscope (AFM) with a high numeric aperture confocal microscope and the facilities for application of radio-frequency (RF) fields for spin manipulation. We verify a sample temperature of <50 K even for strong laser and RF excitation and demonstrate magnetic resonance imaging with a magnetic AFM tip. © *2014 AIP Publishing LLC*. [http://dx.doi.org/10.1063/1.4858835]

I. INTRODUCTION

The nitrogen-vacancy (NV) center in diamond can be utilized as an atomic-size magnetic field sensor with sensitivity on the single spin level. This remarkable capability has spawned great efforts towards applying these sensors to nanoscale magnetic resonance imaging,[1–5] which bears the potential to analyze the structure of complex molecules at the atomic level.[6]

Working towards this goal, the detection of small nuclear spin ensembles from organic molecules on the surface of a bulk diamond containing the NV sensor has been demonstrated.[7,8] The integration of the NV spin sensor into a scanning probe microscope has enabled high precision magnetometry with nanoscale spatial resolution, which has been applied to field mapping of magnetic nanostructures and single electron spin imaging.[9,10] The underlying concept is shown in Fig. 1(a): the NV center is placed at the tip apex of an atomic force microscope (AFM) and scanned over the sample surface. The spin state of the NV center is read out by recording its fluorescence under optical excitation. By positioning the NV probe close to target spins on the sample, a controlled coupling can be realized. The application of radio-frequency (RF) fields allows the coherent manipulation of NV and target spins and therewith the use of sophisticated detection schemes well known from electron paramagnetic resonance (EPR) experiments.[11]

The spin dependent contrast in the NV center fluorescence can be understood using the energy level scheme shown in Fig. 1(b): The optical ground state is a spin triplet $^3A_2$ with a zero field splitting of 2.87 GHz. The system can be optically excited to the ^3E level and decays via fluorescence at a zero-phonon energy of 637 nm. The $|m = \pm 1\rangle$ states have a competing non-radiative decay channel via metastable singlet states, therefore the fluorescence intensity of the ± 1 manifold is decreased compared to the $m = 0$ subsystem. Moreover, the decay channel via the singlet state leads into the $m = 0$ state, resulting in an efficient spin polarization by optical cycling. These two effects enable optical detection of the magnetic resonance (ODMR) of the NV. In an external magnetic field the ± 1 spin states show a Zeeman splitting, resulting in a change of the transition frequencies within the optical ground states. Due to the long coherence time of the NV, which can reach the ms-range for pure diamond,[12] these transition frequencies can be measured with a very high precision, leading to an extremely high magnetic field sensitivity of the NV sensor.[1]

The placement of the NV sensor spin at the apex of a scanning tip can be realized in different ways: one possibility is to graft a diamond nanocrystal (diameter typically ~10 nm) containing a single NV center onto a standard tip.[3,9,13] Alternatively, monolithic scanning probes consisting of diamond nanopillars with an individual NV center implanted at the apex can be fabricated.[5] The latter approach provides longer NV spin coherence times and thus a higher magnetic field sensitivity (owing to the high crystal quality of the nanopillars) as well as an higher optical collection efficiency due to waveguiding. A third possibility is an inverted geometry, where the NV center is situated close to the surface of a high-purity bulk diamond, while the target spin is attached to the scanning tip.

Previous experimental demonstrations of scanning-NV magnetometry have been performed under ambient conditions, a remarkable feat enabled by the unique properties of the NV center. However, many interesting sample systems require a low temperature and ultra-high vacuum (UHV) environment. The relaxation lifetime of molecular electron spins, which, in many cases, limits the applicability of sophisticated

a)Electronic mail: m.ternes@fkf.mpg.de

 © 2014 AIP Publishing LLC

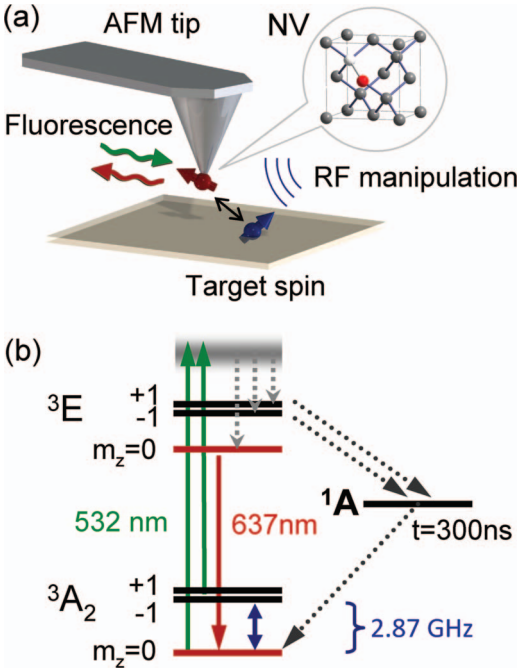

FIG. 1. (a) Measurement principle: the NV spin sensor is attached to an AFM tip and positioned near the target spin. Both spins can be manipulated by RF pulses, spin state readout is achieved via the NV fluorescence. The inset shows the structure of the NV center, where grey spheres represent carbon atoms, red nitrogen, and white the vacancy. (b) Energy level scheme of the NV center.

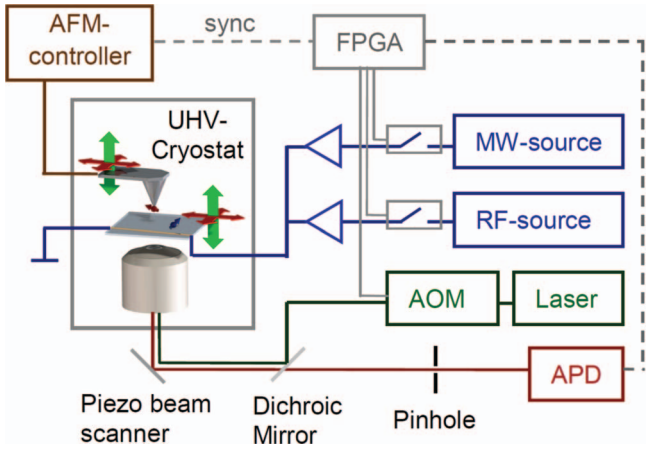

FIG. 2. Scheme of the experimental setup. AFM scanner and front lens of the confocal microscope are mounted in an UHV cryostat, RF fields can be applied to the sample via high frequency transmission lines. 3D positioners for tip and sample allow the alignment of the AFM with the optical focus. Pulsed experiments with nanosecond time resolution are controlled by the FPGA.

ESR-protocols, is typically enhanced by orders of magnitude at liquid helium temperature.[14,15] The study of single molecules in a well-controlled environment requires UHV conditions to avoid sample contamination and has been impossible in existing setups operating under ambient conditions.

II. SYSTEM DESIGN

A. System overview

In this article we describe the design of a combined confocal and atomic force microscope for NV-magnetometry operating at low temperature in UHV. The experimental setup is schematically shown in Fig. 2. The microscope head, containing the AFM scanner, sample, and the optical element for focusing and light collection, is mounted in an UHV-cryostat. Since optical focus, sample, and AFM tip have to be aligned relative to each other, nanoscale positioning with six degrees of freedom is required. In our system, the tip and the sample are independently movable in 3 dimensions, while the optical element is fixed. Tip and sample holder can be exchanged *in situ* and are designed such that the NV sensor spin can be placed at the scanning tip (in a diamond nanocrystal or a nanopillar) as well as in the sample (inverted geometry) with minor modifications.

We use a diode-pumped solid-state laser (532 nm) to optically excite the NV and detect the fluorescence by an avalanche photo-diode (APD). Two RF-sources are employed for NV (frequency range 1–4 GHz) and target spin manipulation (70–450 MHz). Sophisticated ODMR experiments require sequences of laser and RF-pulses with nanosecond time resolution. This is achieved by RF-switches and an acousto-optical modulator (AOM), controlled by a field programmable gate array (FPGA) with 2.5 ns time resolution. The RF-pulses are coupled into a waveguide on the sample via an impedance matched transmission line.

The atomic force microscope is controlled by a commercial electronics system (Nanonis SPM Controller, Specs Zurich), which is synchronized with the ODMR control system for combined experiments.

B. Optical access

The key challenge in designing the microscope head is the realization of the optical access to the scanning tip with high collection efficiency. Similar challenges were addressed in various experimental setups by using high numeric aperture (NA) objective lenses,[9,16] optical fibers,[17] single lenses,[18,19] or parabolic or ellipsoidal mirrors.[20,21] While in our case tip and sample are at low temperature, the optical element can, in principle, be positioned outside the cryostat. This would require relatively long working distances and windows between the sample and lens, which reduces the collection efficiency due to a reduced NA and aberrations. We circumvented this issue by integrating the optical element into the microscope head, such that it is also held at low temperature. This approach additionally enables a compact design with small temperature gradients and, therefore, a high mechanical stability, but does require low temperature compatible optical elements.

High NA objective lenses widely used for room temperature experiments typically consist of sophisticated multi-lens systems to correct for aberrations, including doublet and triplet lenses connected by optical cement. At low temperature, the performance of these objectives is strongly reduced due to changes in the diffraction index of the glasses and thermal expansion, which can lead to cracking.

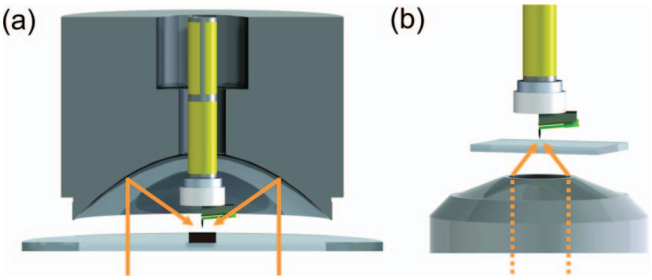

FIG. 3. The two concepts for optical access to the AFM tip. (a) Parabolic mirror. (b) Objective lens.

Single aspheric lenses as in Ref. 19 are more robust and reliable at low temperature, but they show strong chromatic aberrations. As the NV center fluoresces across a rather broad wavelength range (650–750 nm), the collection efficiency of single aspheric lens is found to be insufficient for our purposes.

Parabolic or ellipsoidal mirrors do not show any chromaticity and are fully low temperature compatible. Confocal microscopes using high NA parabolic mirrors have shown spatial resolution close to the diffraction limit under ambient[22] and cryogenic conditions.[23] However, parabolic mirrors need an extremely high manufacturing precision, since small deviations from the ideal parabola shape lead to a strong performance decrease, and feature a poor off-axis performance requiring a precise alignment of the optical setup.[23,24]

Based on these considerations we designed a versatile setup in which an objective lens or, alternatively, a parabolic mirror can be used for illumination and light collection (Fig. 3). When using the parabolic mirror, the sample is supported by a transparent sapphire plate, while the AFM tip is mounted on a piezotube situated in a central bore in the mirror. Alternatively, an objective lens can be mounted beneath the sample. In this geometry we are limited to transparent samples, but it enables the use of lenses with a short working distance and thus a high collection efficiency.

C. Microscope head

We constructed a microscope head combining tip, sample, optical elements, and the required nanopositioners in a compact and rigid assembly. While tip and sample can be moved independently in 3 dimensions, the optical element is fixed to guarantee a stable alignment relative to the optical setup outside the vacuum system. The AFM is based on a qPlus-design where the tip is attached to a quartz tuning fork.[25] The oscillation of the tuning fork is read out electrically, which allows an easy integration into the low temperature setup.

The main components of the microscope head are shown in the exploded view depicted in Fig. 4(a). It consists of the tip positioner unit with the AFM scan assembly, the sample positioner, a rigid housing, and the interface plate that connects to the cryostat and holds the wiring. The microscope head is machined from phosphor bronze (92% Cu, 8% Sn) due to its high

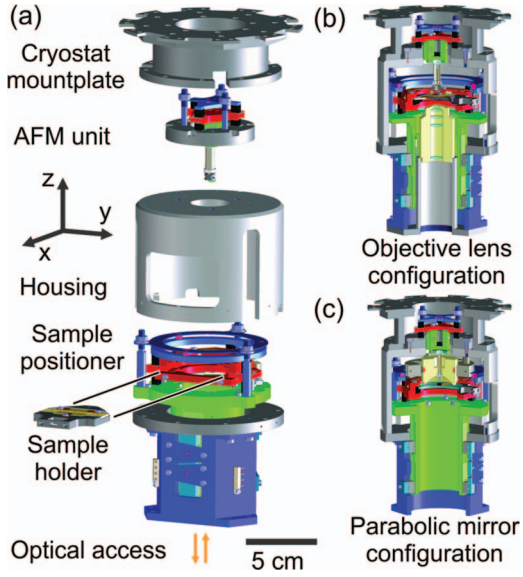

FIG. 4. Model of the microscope head. (a) Exploded view. (b) Cross section with mounted objective lens. (c) Cross section with mounted parabolic mirror. Red: components of the piezo positioners moving in the xy-plane; green: parts moving in z- direction; yellow: optical elements; grey: housing.

thermal conductivity and good machinability. Electrically isolating parts are made from glass-ceramic or sapphire.

The sample positioner unit is a combination of three homebuilt piezomotors based on the slip-stick principle.[26] They allow coarse positioning of the sample within a range of 15 mm in the z-direction and 5 mm in x and y. The positioner unit features a 50 mm bore in the center allowing optical access to the sample from underneath. The objective lens can be mounted in this bore (Fig. 4(b)), or alternatively a parabolic mirror can be placed above the sample (Fig. 4(c)).

The AFM unit consists of homebuilt slip-stick piezomotors for coarse positioning in the xy-plane (range 3 mm) and a commercial positioner (attocube) for coarse z-motion (6.5 mm travel range). The AFM tip is scanned over the sample using a segmented piezotube that enables three-dimensional positioning with pm accuracy over a range of 1 μm. The tuning fork carrying the tip is mounted on a tip holder attached to the scan piezo. We emphasize that both sample and tip can be exchanged *in situ* without warming up the system or breaking the vacuum.

D. Cryostat and UHV-system

The microscope head is mounted to the cold plate of a commercial helium bath-cryostat (CryoVac) integrated into an UHV system (Fig. 5). The microscope head is surrounded by two radiation shields, connected to a 9.6 l liquid helium and a 30 l liquid nitrogen reservoir. The optical setup is mounted on an optical board placed beneath the vacuum chamber. The light accesses the microscope head through viewports (Fused silica and BK7, AR-coating 525–975 nm) in the base of the UHV chamber and the radiation shields. This free-beam access has lower transmission losses compared to widely used fiber-based approaches and, therefore, improves the photon count rate detected from single NV centers.

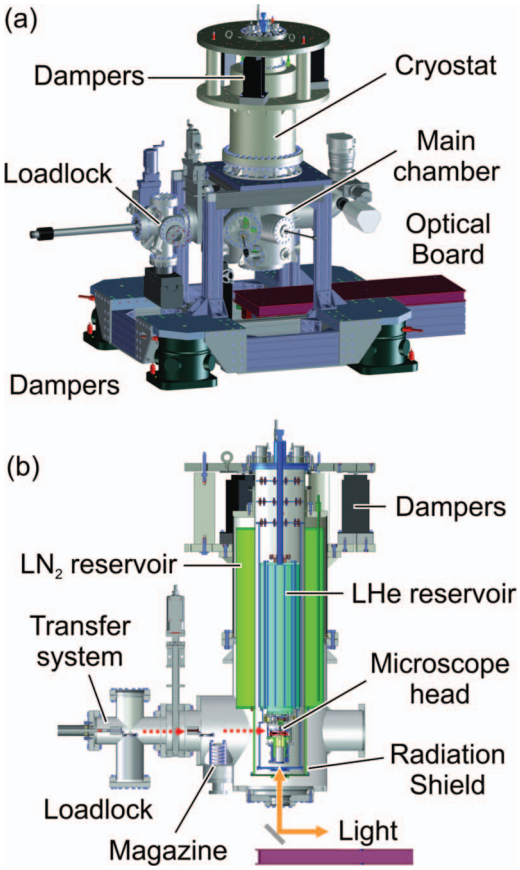

FIG. 5. (a) Model of the vacuum setup with cryostat and optical board (red) for the confocal microscope. (b) Cross section of the setup. Red dotted arrows indicate the sample transfer between loadlock chamber, sample magazine, and microscope head. The orange arrow illustrates the beam path for excitation and fluorescence light through viewports in the UHV chamber and radiation shields.

All electrical wires leading to the microscope head are thermally anchored to the cryostat baffles to reduce the heat load on the head. Therewith, a base temperature of $T_B = 4.7$ K and a standing time of 3–6 days, depending on the operational conditions, is reached.

The vacuum system consists of a main chamber, containing the cryostat and microscope head, and a smaller load-lock and preparation chamber. Both chambers can be independently pumped by a combination of turbo and ion getter pumps to a base pressure of 10^{-10} mbar. Samples and tips can be moved with a mechanical transfer mechanism between the chambers. A wobblestick mounted on the main chamber is used to shuttle samples and tips between the microscope head and a storage magazine. This mechanism enables fast sample and tip exchanges while keeping the microscope head at low temperature. The load-lock and preparation chamber is equipped with ports for Knudsen cell evaporators, leak valves, or heaters enabling sample cleaning and molecule deposition.

To achieve a sub-nm vibration level for AFM experiments the system is equipped with two sets of damping elements: active dampers (TMC Stacis 2100) at the base of the machine decouple the system from building vibrations in a frequency range of 0.6–100 Hz. A passive damping stage (Newport I-500) between the UHV-chamber and the cryostat insert efficiently suppresses higher frequency vibrations (>10 Hz). Although this second damping stage is placed between the optical element in the microscope head and the optical setup outside of the chamber, we do not see any effect on the optical stability.

E. Sample holder design

We designed the sample holder to enable a fast and reliable sample exchange under vacuum conditions and to provide an efficient RF access for spin manipulation. The latter is realized by waveguides fabricated on the sample holder that are contacted by spring-loaded connectors integrated into the sample stage (Figs. 6(a)–6(c)).

A schematic of the sample holder can be seen in Fig. 6(b); the version shown is for experiments using an objective lens. Measurements using a parabolic mirror utilize an adapted version. A base part made from phosphor bronze or titanium supports a circuit board with a coplanar waveguide. In the center a thin (170 μm) plate of sapphire with a similar waveguide is mounted. This sapphire supports the actual sample, e.g., a diamond membrane. The high thermal conductivity of sapphire at low temperature enables an efficient cooling of the sample. To implement optical access of the objective to the diamond, the sapphire has a small aperture beneath the sample. The RF access to the sample is realized by a microfabricated waveguide or a thin wire spanned over the surface. The different waveguides on the sample holder are connected by wire-bonding. For handling the samples in the vacuum system the sample holder has an interface to the wobble stick transfer head.

To provide a mechanically stable mount for AFM experiments the holder is fixed in the sample stage by a spring mechanism (Fig. 6(b)): The sample holder rests on 3 pads in the sample stage, while it is clamped by 3 spring-loaded ruby balls. The ruby balls snap into dents in the sample holder, which provides a high reproducibility of the sample position.

The coupling between the waveguides on the sample holder and the transmission lines in the microscope head is

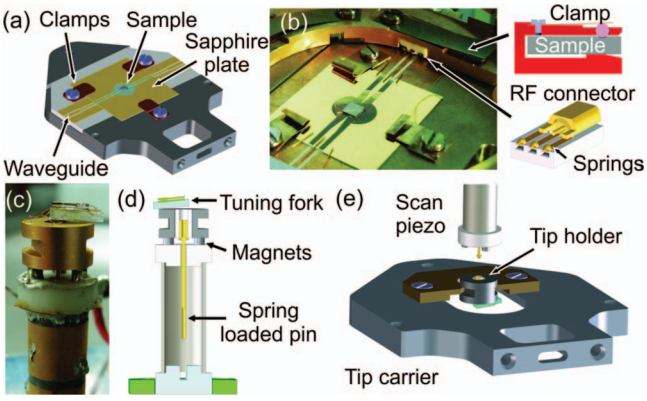

FIG. 6. (a) Model of the sample holder for measurements using the objective lens (b) Photography of the sample holder in the sample stage with schematic views of the clamping mechanism and RF contacts. (c) Photograph of the magnetic tip holder with tuning fork sensor. (d) Cross section of the tip holder revealing the central spring contact for the tuning fork signal. (e) Illustration of the tip exchange: the tip holder can be inserted in a carrier with the dimensions of the sample holder.

realized by homebuilt spring-loaded contacts (Fig. 6(b)). They are assembled from commercially available MiniSMP connectors, a glass-ceramic body, and 3 CuBe springs with Cu half spheres glued to it. The dimensions of these connectors, as well as those of the waveguides on the sample holder, are chosen to give a characteristic impedance close to 50 Ohms in order to provide high RF transmission and low reflections. The overall attenuation of the spring contacts and the sample holder waveguides is typically −5 dB at 3 GHz.

F. AFM assembly

To perform *in situ* tip exchange, we designed a magnetic tip holder that provides a rigid mechanical connection to the scan piezo and the two electrical contacts needed for the tuning fork excitation and readout. A photograph and a cross-sectional view can be seen in Figs. 6(c) and 6(d). The stationary part is glued to the piezotube and consists of a glass-ceramic body with three CoSm-magnets in a triangular arrangement around a central spring-loaded pin. The exchangeable part is assembled from a gold-plated body of magnetizable steel and a central contact isolated by an alumina tube. The tuning fork, supported by a sapphire holder, is glued on top of the steel part. One electrode of the tuning fork is connected via the central contact to the spring-loaded pin in the piezotube, the other one via the steel body to the magnets. The central pin and one of the magnets are contacted by wires inside the piezotube.

The force between the magnets and the magnetic steel piece is much stronger than the opposing force generated by the spring loaded pin, resulting in a rigid and reliable connection. For tip exchange, a tip carrier can be inserted into the sample stage. It has an aperture in the center that fits the tip holder geometry (Fig. 6(e)). For exchanging the tip, the carrier is moved in 3 dimensions such that the tip holder is locked in the carrier. The scan piezo can then be retracted while leaving the tip holder in the carrier. The mounting of fresh tips works in an analogous way; the conical pin in the piezotube and the funnel-like shape of the central contact in the tip holder lead to a self-centering of the tip holder relative to the piezotube.

The excitation of the tuning fork is carried out electrically by applying an alternating voltage at its resonance frequency directly to one of its electrodes, while the second electrode is used to read out the tuning fork oscillation. To avoid crosstalk due to the parasitic capacitance between the two channels we employ a compensation scheme similar to that described in Ref. 27. The tuning fork signal is amplified by a home-built transimpedance amplifier with 10^8 V/A gain (based on OPA657) integrated into the microscope head and working at low temperature.

III. PERFORMANCE

A. Confocal imaging and optically detected magnetic resonance

For the performance of the NV-magnetometer the efficiency of the optical access to the tip in the cryostat is crucial. As discussed above, a parabolic mirror as well as an objective lens offers certain advantages in low temperature experiments and both can be integrated into our setup. Since parabolic mirrors available to date were found to be insufficient in size or quality, we will focus in the following on the approach using a low temperature objective lens. Nevertheless, a mirror-based approach might be an interesting alternative for future experiments.

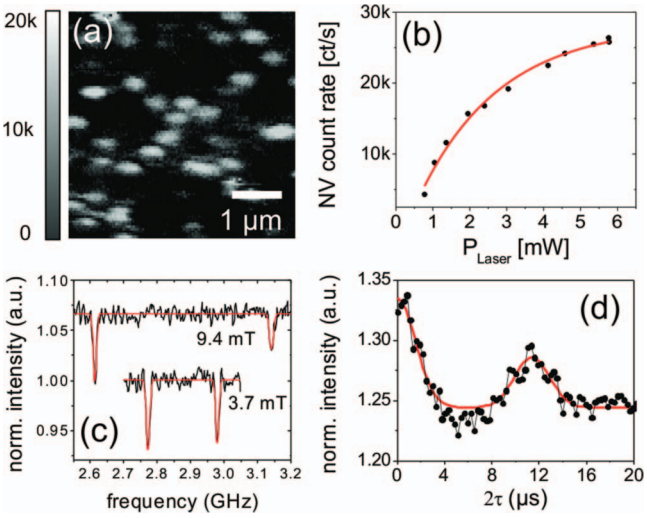

FIG. 7. ODMR-measurements on single NVs implanted with 5 keV in a 20 μm diamond membrane. (a) Confocal image. (b) Saturation curve. (c) ODMR-spectra for two magnetic fields. (d) Spin echo revealing ^{13}C-induced collapse and revival and a coherence time of 20 μs.

For our experiments we used an objective lens with a numeric aperture of 0.82 (Partec), which is widely used in low temperature experiments. Figure 7(a) shows a typical confocal image of NV centers in a bulk diamond sample obtained at 4.7 K in UHV. As can be seen in the saturation curve (Fig. 7(b)), the maximum count rate for a single NV is around 25 kcts/s. This value is significantly lower than the ∼100 kcts/s obtained with higher-quality air objective lenses under ambient conditions, but corresponds well to values reported for low temperature experiments.[28] The performance of the objective is found to be unchanged even after several thermal cycles between 4.7 K and 400 K, indicating that degradation caused by thermal strain is negligible.

Representative ODMR-spectra for a single NV are shown in Fig. 7(c); for two different external magnetic fields the NV fluorescence is recorded for varying microwave frequency. The dips in the fluorescence correspond to the resonance of the microwave field with $|m = 0\rangle \rightarrow |-1\rangle$ and $|0\rangle \rightarrow |+1\rangle$ spin transitions, respectively.[3] An example of coherent spin manipulation can be seen in Fig. 7(d), where the spin echo of a single NV center is shown. The "collapse" and subsequent revival of the spin echo signal is induced by an interaction between the NV and the C^{13} nuclear spin bath.[29]

B. Laser and RF heating

An important question in a low temperature setup is the local temperature of the probed sample region. Although the microscope head is cooled to 4.7 K, the temperature in the

laser focus might be significantly higher due to local heating, especially when strong radio-frequency fields are additionally applied. Since conventional temperature sensors are too far away from the focal region, we employed an optical temperature measurement based on the fluorescence of Cr^{3+} color centers in sapphire.[30,31] The Cr^{3+} center features a strong fluorescence emission around 693 nm due to radiative transitions from the ^2E to the $^4A_2$ manifold. Since the ^2E degeneracy is partially lifted by the crystal field, the zero-phonon line is split into two emission lines (referred to as R_1 and R_2) separated by ~2 nm. The occupation of the ^2E-levels is governed by the Boltzmann distribution, and, therefore, the intensity ratio between both lines is strongly temperature dependent. To evaluate the temperature from an intensity analysis the strong polarization of the light emission has to be taken into account; the intensity ratio depends on the angle of the sapphire c-axis relative to the polarization direction of the detector.[32]

Since Cr^{3+} is an abundant impurity in the sapphire plates used as support in our sample holders, we estimated the local temperature by analyzing their fluorescence with a grating spectrometer. The analysis of the spectra is complicated by the *a priori* unknown angle between the sapphire c-axis and the spectrometer and the fact that the objective lens does not maintain the polarization direction of the transmitted light at low temperature. To account for these effects, we measured spectra at different base temperatures (T_B = 4.7 K, 77 K, 300 K) and with different polarization directions of the excitation laser. The angle between the sapphire c-axis and the spectrometer axis we inferred from the reference spectra at T_B = 300 K and the polarization dependence published in Ref. 32. For the low temperature measurements we estimated the rotation of polarization caused by the objective lens relative to the room temperature measurement by the dependence on the laser polarization. Under the assumption that the fluorescence light undergoes the same rotation we corrected the measured intensity ratios for the polarization effect and were therewith able to compare the results for different temperatures. By assuming a simple Boltzmann law we calculated the approximate temperature.

Figure 8 shows the acquired fluorescence spectra with the estimated temperature. At liquid helium temperature we measured with and without strong microwave irradiation to account for RF heating. The laser power was in all measurements set to 2.5 mW, the RF transmitted through the sample waveguide had an approximate power of 10 mW.

At liquid nitrogen cooling (T_B = 77 K) without applied RF our analysis yielded $T = (75 \pm 5)$ K, verifying the applicability of our approach. The results at liquid helium cooling (T_B = 4.7 K) with and without RF transmission differ significantly. The spectrum without applied RF shows only a single R_1 line, the R_2 is frozen out implying negligible heating effects due to laser heating.[30] With applied RF field R_2 is clearly expressed, the local sample temperature is increased to about T = 45 K.

Typical ODMR-experiments are performed with pulsed RF excitation with lower time-averaged power; for realistic pulse sequences we, therefore, expect $T \approx 30$ K, depending on the RF duty cycle. In future experiments the effective temperature could be reduced by improving the thermal anchoring of the sample or by using RF transmission lines thermally decoupled from the sample.

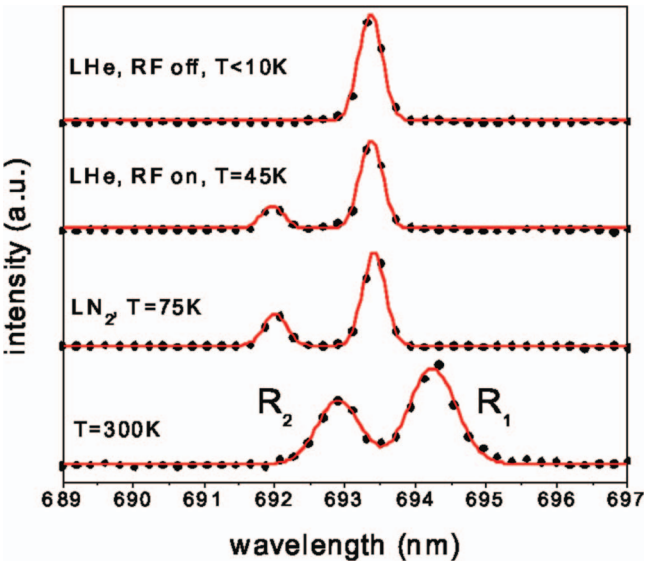

FIG. 8. Representative fluorescence spectra of Cr3+ color centers in sapphire for different temperatures. The intensity ratios of the two lines allow an estimate of the local temperature.

C. Atomic force microscopy

To verify the performance of the AFM we imaged a Au film on glass as a benchmark sample (Fig. 9). The sample was cleaned by flame annealing under ambient conditions and subsequently introduced into the vacuum system. We used a commercially available silicon tip, which we transferred to our tuning fork sensor (stiffness k = 1800 N/m) with a micromanipulator. The measurement is carried out in the non-contact regime with frequency modulation feedback, an oscillation amplitude of 1 nm, and a set point of $\Delta f = -6$ Hz (free oscillation frequency f_0 = 30 300 Hz). The atomic steps on the Au(111) surface are clearly resolved. The z-noise during scanning is ~20 pm (peak-peak) in the bandwidth of 1–100 Hz, verifying the high mechanical stability of the microscope head.

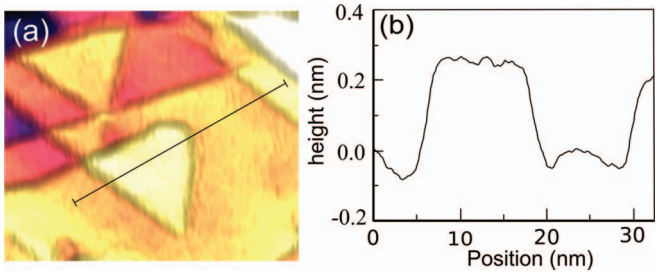

FIG. 9. (a) AFM topography (40 × 30 nm) of Au on glass. Image acquired in the non-contact mode with FM-feedback. (b) Line profile revealing atomic steps of the Au surface.

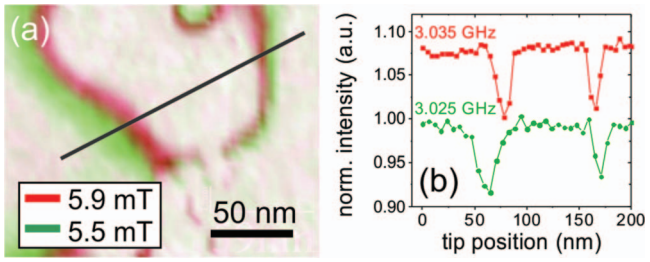

FIG. 10. Demonstration of magnetic resonance imaging. (a) A magnetic tip is scanned over a NV center close to the diamond surface. For continuous optical excitation and applied constant RF-field close to resonance, the NV fluorescence is plotted as a function of tip position. The image is composed of two subsequent measurement runs with different RF detuning. (b) Line profiles along the black line for the two RF frequencies.

D. Magnetic resonance imaging

To demonstrate NV-based magnetic field mapping and the interplay of confocal microscopy, magnetic resonance spectroscopy, and atomic force microscopy, we employed the NV spin sensor to image the local magnetic field produced by a magnetic AFM tip. The tip is scanned over a single NV close to the surface of a bulk diamond (depth $\sim$ 8 nm), while simultaneously a microwave field with a constant frequency close to the NV resonance frequency is applied. This represents a crude example of scanning NV magnetometry in the inverted geometry with a stationary NV center and a scanned target system (here the tip itself). Since the tip creates a strong magnetic field gradient, the field at the NV position and, therefore, the resonance frequencies (compare Fig. 7(c)) depend strongly on the tip position. When plotting the fluorescence intensity as a function of tip position, areas where the applied microwave is on resonance with the NV appear as dark lines (Fig. 10). The structures in the fluorescence map can be interpreted as equipotential lines of the magnetic field created by the tip. For a radially symmetric field the lines form ring-like structures.[3,33] In our measurements the tip is probably composed of different magnetic particles or domains, leading to the rather complex field distribution seen in the image.

The spatial resolution in the presented measurements is around 20 nm and is limited by the field gradient produced by the magnetic tip and the power-broadened transition linewidth. Increasing the spectral resolution by suitable pulse sequences (e.g., Ramsey spectroscopy) and engineering steeper field gradients will improve the spatial resolution for NV-based magnetic resonance imaging. By employing high-order dynamic decoupling and field gradients similar to the ones reached in MRFM (on the order of 10^6 T/m[34]), a spatial resolution of 0.1 nm might be achievable.[1]

IV. CONCLUSION AND OUTLOOK

We described the design of a scanning probe spin sensor based on the NV center in diamond operating at low temperature in ultra-high vacuum. The performance of the instrument was demonstrated by presenting ODMR experiments on single NV centers, high resolution AFM-measurements, and magnetic resonance imaging on the nanoscale. The reported optical count rate of single NV centers is an order of magnitude lower than that commonly achieved under ambient conditions, but can be improved in future experiments by employing diamond nanostructures serving as photon waveguides.[5] The extremely high sensitivity of the NV center, in combination with the low temperature UHV environment, will allow spin sensing of individual electron and potentially even single nuclear spins on the nanoscale. Ultimately, this technique might allow applying the sophisticated methods of EPR and NMR spectroscopy to single molecules.

ACKNOWLEDGMENTS

We sincerely thank Wolfgang Stiepany for technical support, Andreas Gebhardt and Christoph Damm (Fraunhofer IOF, Jena) for manufacturing a parabolic mirror prototype, Jan Meijer and Sébastien Pezzagna (Ruhr-Universität Bochum) for NV implantation, and Bernd Faltermeier (Carl Zeiss AG) for fruitful discussions. We also express our gratitude to Tobias Staudacher, Matthias Niethammer, and Evangelos Fillis-Tsirakis for experimental support. F. R. and J. W. acknowledge financial support by the EU (Squtec), Darpa (Quasar), BMBF (CHIST-ERA) and contract research of the Baden-Württemberg foundation.

[1] J. M. Taylor, P. Cappellaro, L. Childress, L. Jiang, D. Budker, P. R. Hemmer, A. Yacoby, R. Walsworth, and M. D. Lukin, Nature Phys. **4**, 810 (2008).
[2] C. L. Degen, Appl. Phys. Lett. **92**, 243111 (2008).
[3] G. Balasubramanian, I. Y. Chan, R. Kolesov, M. Al-Hmoud, J. Tisler, C. Shin, C. Kim, A. Wojcik, P. R. Hemmer, A. Krueger, T. Hanke, A. Leitenstorfer, R. Bratschitsch, F. Jelezko, and J. Wrachtrup, Nature (London) **455**, 648 (2008).
[4] L. T. Hall, J. H. Cole, C. D. Hill, and L. C. L. Hollenberg, Phys. Rev. Lett. **103**, 220802 (2009).
[5] P. Maletinsky, S. Hong, M. S. Grinolds, B. Hausmann, M. D. Lukin, R. L. Walsworth, M. Loncar, and A. Yacoby, Nat. Nanotechnol. **7**, 320 (2012).
[6] J. Cai, F. Jelezko, M. B. Plenio, and A. Retzker, New J. Phys. **15**, 013020 (2013).
[7] T. Staudacher, F. Shi, S. Pezzagna, J. Meijer, J. Du, C. A. Meriles, F. Reinhard, and J. Wrachtrup, Science **339**, 561 (2013).
[8] H. J. Mamin, M. Kim, M. H. Sherwood, C. T. Rettner, K. Ohno, D. D. Awschalom, and D. Rugar, Science **339**, 557 (2013).
[9] L. Rondin, J. P. Tetienne, P. Spinicelli, C. Dal Savio, K. Karrai, G. Dantelle, A. Thiaville, S. Rohart, J. F. Roch, and V. Jacques, Appl. Phys. Lett. **100**, 153118 (2012).
[10] M. S. Grinolds, S. Hong, P. Maletinsky, L. Luan, M. D. Lukin, R. L. Walsworth, and A. Yacoby, Nature Phys. **9**, 215 (2013).
[11] A. Schweiger and G. Jeschke, *Principles of Pulsed Electron Paramagnetic Resonance* (Oxford University Press, 2005).
[12] G. Balasubramanian, P. Neumann, D. Twitchen, M. Markham, R. Kolesov, N. Mizuochi, J. Isoya, J. Achard, J. Beck, J. Tissler, V. Jacques, P. R. Hemmer, F. Jelezko, and J. Wrachtrup, Nature Mat. **8**, 383 (2009).
[13] A. Cuche, A. Drezet, J. F. Roch, F. Treussart, and S. Huant, J. Nanophotonics **4**, 043506 (2010).
[14] R. Sessoli, D. Gatteschi, A. Ganeschi, and M. A. Novak, Nature (London) **365**, 141 (1993).
[15] H. Sato, S. E. Bottle, J. P. Blinco, A. S. Micallef, G. R. Eaton, and S. S. Eaton, J. Magn. Res. **191**, 66 (2008).
[16] I. Gerhardt, G. Wrigge, P. Bushev, G. Zumofen, M. Agio, R. Pfab, and V. Sandoghdar, Phys. Rev. Lett. **98**, 033601 (2007).
[17] N. J. Watkins, J. P. Long, Z. H. Kafafi, and A. J. Mäkinen, Rev. Sci. Instrum. **78**, 053707 (2007).
[18] J. G. Keizer, J. K. Garleff, and P. M. Koenraad, Rev. Sci. Instrum. **80**, 123704 (2009).
[19] K. Kuhnke, A. Kabakchiev, W. Stiepany, F. Zinser, R. Vogelgesang, and K. Kern, Rev. Sci. Instrum. **81**, 113102 (2010).
[20] S. Hoppe, G. Ctistis, J. J. Paggel, and P. Fumagalli, Rev. Sci. Instrum. **76**, 063704 (2005).

[21]J. Steidtner and B. Pettinger, Rev. Sci. Instrum. **78**, 103104 (2007).
[22]J. Stadler, C. Stanciu, C. Stupperich, and A. J. Meixner, Opt. Lett. **33**, 681 (2008).
[23]A. Drechsler, M. Lieb, C. Debus, A. Meixner, and G. Tarrach, Opt. Express **9**, 637 (2001).
[24]M. Lieb and A. Meixner, Opt. Express **8**, 458 (2001).
[25]F. J. Giessibl, S. Hembacher, M. Herz, C. Schiller, and J. Mannhart, Nanotechnology **15**, S79 (2004).
[26]G. Mariotto, M. D. Angelo, and I. V. Shvets, Rev. Sci. Instrum. **70**, 3651 (1999).
[27]T. Akiyama, N. F. de Rooij, U. Staufer, M. Detterbeck, D. Braendlin, S. Waldmeier, and M. Scheidiger, Rev. Sci. Instrum. **81**, 063706 (2010).
[28]F. Grazioso, B. R. Patton, and J. M. Smith, Rev. Sci. Instrum. **81**, 093705 (2010).
[29]L. Childress, M. V. Gurudev Dutt, J. M. Taylor, A. S. Zibrov, F. Jelezko, J. Wrachtrup, P. R. Hemmer, and M. D. Lukin, Science **314**, 281 (2006).
[30]W. A. Wall, J. T. Karpick, and B. D. Bartole, J. Phys. C: Solid St. Phys. **4**, 3258 (1971).
[31]M. Marceddu, M. Manca, P. C. Ricci, and A. Anedda, J. Phys.: Condens. Matter **24**, 135401 (2012).
[32]J. He and D. R. Clarke, J. Am. Ceram. Soc. **80**, 69 (1997).
[33]M. S. Grinolds, P. Maletinsky, S. Hong, M. D. Lukin, R. L. Walsworth, and A. Yacoby, Nature Phys. **7**, 687 (2011).
[34]M. Poggio and C. L. Degen, Nanotechnology **21**, 342001 (2010).